Construction of Covalent Organic Framework for Catalysis: Pd/COF-LZU1 in Suzuki−Miyaura Coupling Reaction

San-Yuan Ding,[†] Jia Gao,[†] Qiong Wang,[†,‡] Yuan Zhang,[†] Wei-Guo Song,[‡] Cheng-Yong Su,[§] and Wei Wang[*,†]

[†]State Key Laboratory of Applied Organic Chemistry, College of Chemistry and Chemical Engineering, Lanzhou University, Lanzhou, Gansu 730000, China;

[‡]Beijing National Laboratory for Molecular Sciences (BNLMS); Laboratory for Molecular Nanostructures and Nanotechnology, Institute of Chemistry, Chinese Academy of Sciences, Beijing 100190, China;

[§]School of Chemistry and Chemical Engineering, Sun Yat-Sen University, Guangzhou 510275, China

Ⓢ *Supporting Information*

ABSTRACT: Covalent organic frameworks (COFs) are crystalline porous solids with well-defined two- or three-dimensional molecular structures. Although the structural regularity provides this new type of porous material with high potentials in catalysis, no example has been presented so far. Herein, we report the first application of a new COF material, **COF-LZU1**, for highly efficient catalysis. The easily prepared imine-linked **COF-LZU1** possesses a two-dimensional eclipsed layered-sheet structure, making its incorporation with metal ions feasible. Via a simple post-treatment, a Pd(II)-containing COF, **Pd/COF-LZU1**, was accordingly synthesized, which showed excellent catalytic activity in catalyzing the Suzuki−Miyaura coupling reaction. The superior utility of **Pd/COF-LZU1** in catalysis was elucidated by the broad scope of the reactants and the excellent yields (96−98%) of the reaction products, together with the high stability and easy recyclability of the catalyst. We expect that our approach will further boost research on designing and employing functional COF materials for catalysis.
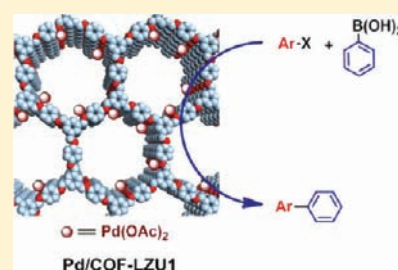
■ INTRODUCTION

As a new type of crystalline porous material, covalent organic frameworks (COFs) are ingeniously constructed with organic moieties linked by strong covalent bonds through the principles of reticular chemistry.[1−7] Similar to those found in crystalline inorganic zeolites[8] and metal organic frameworks (MOFs),[9,10] COF materials possess well-defined and predictable two- or three-dimensional pore structures.[2,3] In comparison with amorphous porous materials, these crystalline porous materials have superior potential in adsorption, in gas storage, and especially in catalysis because of the structural regularity.[11] Indeed, inorganic zeolites have been widely used as catalysts in refining and petrochemical industries.[8,12] Recent research has also demonstrated the possibility of employing MOF materials in catalysis.[13] On the contrary, the catalytic application of COF materials has never been reported so far. Since the first discovery of COF materials in 2005,[2] research in this area has mainly focused on the construction of new COF structures with the aim of increasing the surface area and pore volume,[4−7,14−19] together with some rare examples of applying the synthesized COFs in gas storage[20−22] and photoelectricity.[23−26] In this work, we report the first example of design, synthesis, and application of an imine-linked COF material for catalysis.

As in the cases of other solid catalysts, two basic but important issues should be taken into account in order to design and screen suitable COF candidates for catalytic applications. One is that the COF catalyst must show high stability to thermal treatments, water, and most of the organic solvents. Another is that the COF material should incorporate with catalytic active sites. The most well-known boron-containing COFs linked by boroxine or boronate-ester groups are unfortunately not stable to moisture, although they display high thermal stabilities.[27−29] In contrast, the triazole-,[15] the imine-,[16] and hydrazone-based[30] COF materials, being highly stable in water and most organic solvents, meet the first requirement as robust catalysts. Moreover, it has been well demonstrated[31] in coordination chemistry that the imine-type (Schiff base) ligands are versatile in incorporating a variety of metal ions. This intrigued us to explore the possibility of using imine-linked metal-ion-incorporated COF materials for catalysis. However, the only reported example of imine-linked COF, *i.e.*, COF-300,[16] possesses a three-dimensional diamond structure in which the nitrogen atoms of the imine-bonds are far away from each other (the minimum distance is ∼6.6 Å). This arrangement makes COF-300 less possible to coordinate with metal ions efficiently. Accordingly, we synthesized a new imine-linked COF material (denoted as **COF-LZU1**) with a two-dimensional (2D) layered-sheet structure (Figure 1). The eclipsed layered-sheet arrangement renders the distance of eclipsed nitrogen atoms in adjacent layers as ∼3.7 Å, which makes the synthesized **COF-LZU1** material an ideal scaffold for incorporating a variety of metal ions.
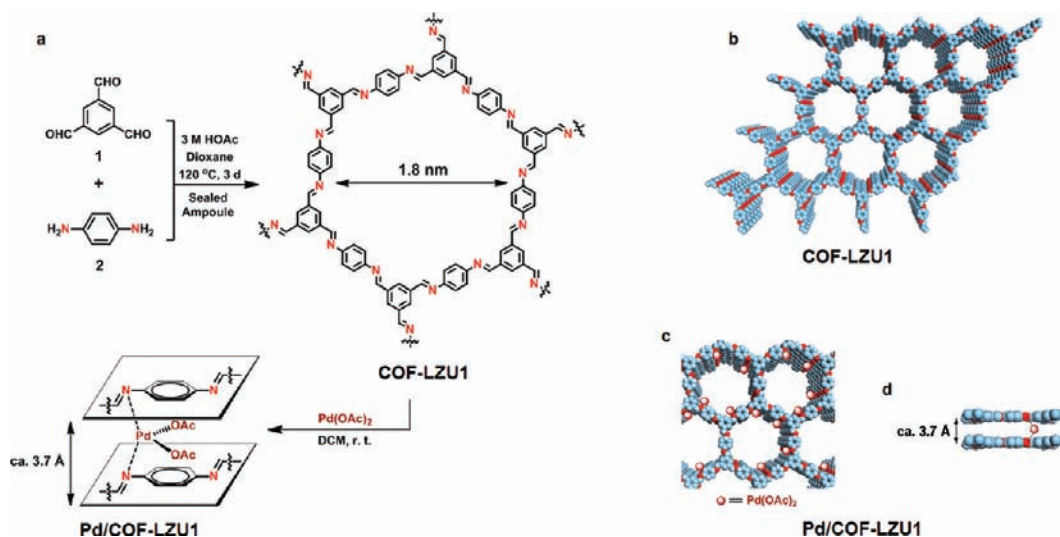
Figure 1. Construction of **COF-LZU1** and **Pd/COF-LZU1**. Schematic representation for the synthesis of **COF-LZU1** and **Pd/COF-LZU1** materials (a). Proposed structures of **COF-LZU1** (b) and **Pd/COF-LZU1** (c, d) possessing regular microporous channels (diameter of ∼1.8 nm), simulated with a 2D eclipsed layered-sheet arrangement. C: blue, N: red, and brown spheres represent the incorporated Pd(OAc)$_2$. H atoms are omitted for clarity.

As an example, the palladium(II)-coordinated COF material (denoted as **Pd/COF-LZU1**) was facilely synthesized via a simple treatment of **COF-LZU1** with Pd(OAc)$_2$ at room temperature. The structural preservation and robust Pd(II)-incorporation of the synthesized **Pd/COF-LZU1** was verified by powder X-ray diffraction (PXRD), solid-state NMR spectroscopy, and X-ray photoelectron spectroscopy (XPS). We then applied the **Pd/COF-LZU1** material in catalyzing the Suzuki–Miyaura coupling reaction, an important reaction for the formation of C–C bonds.[32] The excellent catalytic activity of **Pd/COF-LZU1** was elucidated by the broad scope of the reactants and the excellent yields (96–98%) of the reaction products, together with the high stability and easy recyclability of the catalyst. In comparison with that of zeolites or MOFs, the superior activity of **Pd/COF-LZU1** material should be attributed to its unique structure, which offers efficient access to the active sites and fast diffusion for the bulky products.

■ EXPERIMENTAL SECTION

Synthesis of COF-LZU1. 1,3,5-Triformylbenzene **1** (48 mg, 0.30 mmol) and 1,4-diaminobenzene **2** (48 mg, 0.45 mmol) were weighed into a vial and dissolved in 3.0 mL of 1,4-dioxane. The mixture was transferred into a glass ampule (volume ∼20 mL with a body length of 18 cm and a neck length of 9 cm), and to the mixture was added 0.6 mL of 3.0 mol/L aqueous acetic acid. The glass ampule was flash frozen in a liquid nitrogen bath, evacuated to an internal pressure of 19 mbar and flame-sealed, reducing the total length by ∼10 cm. Upon warming to room temperature, the suspension was placed in an oven at 120 °C and left undisturbed for 3 days, yielding a yellow solid along the tube which was isolated by centrifugation, washed with N,N-dimethylformamide (3 × 10 mL) and tetrahydrofuran (3 × 10 mL), and dried at 80 °C under vacuum for 12 h to yield **COF-LZU1** as a yellow-colored powder (72 mg, 90% yield). Anal. Cald for (C$_6$H$_4$N)$_n$: C 80.00; H 4.44; N 15.55. Found: C 76.34; H 4.61; N 14.20. IR (powder, cm^{-1}) 3382, 2864, 1694, 1618, 1496, 1444, 1250, 1146, 968, 880, 832, 730, 685. PXRD [2θ (relative intensity)] 4.70 (100), 8.05 (8), 9.47 (3), 12.45 (2), 26.22 (3).

Synthesis of Pd/COF-LZU1. Palladium acetate (45 mg, 0.2 mmol) was dissolved in 10 mL of dichloromethane, and then **COF-LZU1** (165 mg) was added. The mixture was kept stirring for 24 h at

room temperature. The resulting solid was isolated by centrifugation, washed with dichloromethane using Soxhlet extraction for 24 h, and then dried at 80 °C under vacuum for 12 h to yield **Pd/COF-LZU1** as a brown-colored powder (166 mg, 79% yield). The Pd content was 7.13% as determined by ICP. Anal. Cald for 0.077·nPd(OAc)$_2$@(C$_6$H$_4$N)$_n$: C 70.57; H 4.16; N 13.05. Found: C 66.04; H 3.97; N 12.51. IR (powder, cm^{-1}) 3339, 2862, 1696, 1617, 1495, 1411, 1250, 1147, 968, 881, 836, 730, 685. PXRD [2θ (relative intensity)] 4.68 (100), 8.18 (6), 9.35 (4).

General Procedure for the Suzuki–Miyaura Coupling Reactions. In a typical run for catalytic activity test of **Pd/COF-LZU1**, aryl halide (1.0 mmol), phenylboronic acid (183 mg, 1.5 mmol), potassium carbonate (276 mg, 2.0 mmol), and **Pd/COF-LZU1** (7.5 mg, 0.5 mol %) were added to 4 mL of p-xylene. The reaction mixture was stirred at 150 °C under reflux at ambient atmosphere. After the reaction was completed (monitored by TLC), the mixture was centrifugated, and the solid was washed with dichloromethane (3 × 5 mL). The combined organic phase was washed with water (20 mL) to remove potassium carbonate. The organic phase was then evaporated under reduce pressure to leave the crude products which were further purified by column chromatography over silica gel to obtain the desired products. In a recycle test, p-nitrobromobenzene (202 mg, 1.0 mmol), phenylboronic acid (183 mg, 1.5 mmol), potassium carbonate (276 mg, 2.0 mmol), and **Pd/COF-LZU1** (15 mg, 1.0 mol %) in 4 mL of p-xylene were used. After each cycle, the catalyst was dried and then used directly without any further treatment.

Other detailed experimental descriptions can be found in the Supporting Information [SI].

■ RESULTS AND DISCUSSION

As shown in Figure 1a, the imine-linked **COF-LZU1** material could be reproducibly synthesized by heating the suspension of 1,3,5-triformylbenzene **1** and 1,4-diaminobenzene **2** in a mixture of 1,4-dioxane and aqueous acetic acid within a flame-sealed glass ampule (see SI for details). The synthesized **COF-LZU1** material is insoluble in water or common organic solvents (such as N,N-dimethylformamide, tetrahydrofuran, dimethyl sulfoxide, acetone, trichloromethane, etc.). The Fourier transform infrared (FT-IR) spectrum of **COF-LZU1** shows a strong C═N stretch at 1618 cm^{-1} (Figure S1, SI), indicating the formation of
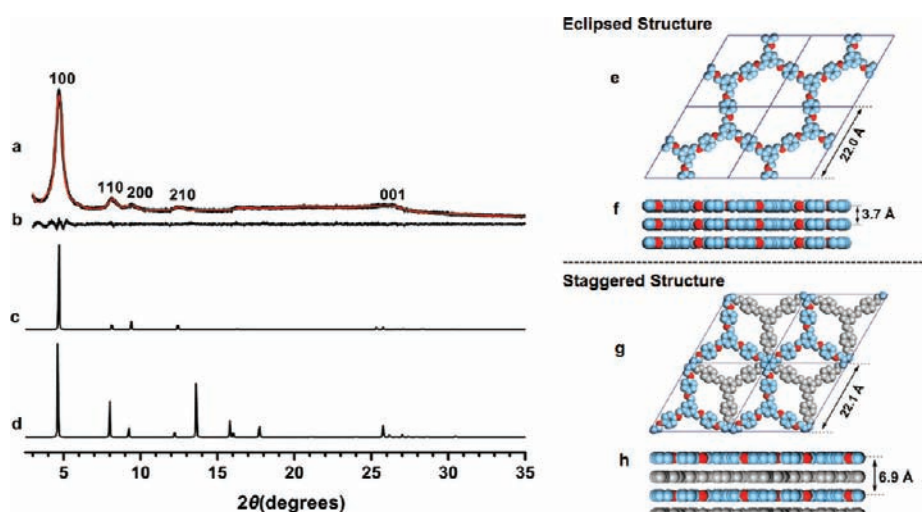
Figure 2. Left: (a) Observed PXRD pattern (black, the major reflections are assigned) and refined modeling profile (red) of **COF-LZU1**. (b) Difference plot between the observed and refined PXRD patterns. (c) Simulated PXRD pattern for an eclipsed structure. (d) Simulated PXRD pattern for a staggered structure. Right: (e,f) Eclipsed structure with the unit cell parameters indicated. (g,h) Staggered structure with the unit cell parameters indicated. C: blue, N: red, and H atoms are omitted for clarity. For the staggered structure, alternating gray layers with undefined atoms are presented for better visuality.

imine bonds. Meanwhile, the aldehyde (1695 cm^{-1}) and amino (3415 cm^{-1}) bands of **COF-LZU1** were greatly attenuated in comparison with those of the starting materials **1** and **2** (Figure S1, SI), which offers further evidence for the formation of imine bonds via the condensation of aldehyde **1** and primary amine **2**. The residual signals at these wavenumbers correspond to the terminal aldehyde and amino groups at the edges of the **COF-LZU1** material, respectively.

Powder X-ray diffraction (PXRD) analysis with Cu Kα radiation was used to determine the crystalline structure of **COF-LZU1**. The PXRD pattern (Figure 2a, black) indicates that **COF-LZU1** is a microcrystalline material with a long-range structure depicted in Figure 1b (see details in e and f of Figure 2). The most intense peak with d spacing of 18.78 Å is attributed to the (100) diffraction, while other diffraction peaks with d spacings of 10.98, 9.33, 7.11, and 3.45 Å are attributed to the (110), (200), (210), and (001) facets, respectively. Furthermore, no diffraction peaks from the starting material **1** or **2** could be observed (Figure S8, SI), indicating the sole formation of crystalline **COF-LZU1** material. The lattice modeling and Pawley refinement (see SI for details) of **COF-LZU1** were conducted with the Materials Studio (ver. 4.4) suite of programs.[33] The most probable structure of **COF-LZU1** was simulated, analogous to that of COF-5,[2] as the eclipsed layered-sheets using the space group of $P6/m$ with the optimized parameters of $a = b = 22.040$ (± 0.228) Å and $c = 3.729$ (± 0.040) Å (e and f of Figure 2). To our delight, the calculated PXRD pattern (Figure 2c) of this hexagonal unit cell matched the experimental profile in peak positions and relative intensities quite well, with wR_p of 4.70% and R_p of 3.68%, respectively. An alternative staggered model was also predicted (Figure 2g). However, the simulated PXRD pattern (Figure 2d) did not match the observed data.[34] In order to verify the preferred eclipsed-structure of **COF-LZU1**, we further applied the force-field-based molecular mechanics calculations[33] to compare the total energies of both models against the stacking distances[35] (see SI for details). The eclipsed model showed a distinct energetic preference to the staggered model (Table S2 and Figure S10, SI). Meanwhile, the layer distance (3.6 Å) for the eclipsed structure at

low-energy minima is very close to the c value derived from Pawley refinement (3.7 Å). In comparison, the staggered model gives the layer distance of 3.3 Å at low-energy minima. Therefore, the structure of **COF-LZU1** should preferably be determined as the eclipsed layered-sheet arrangement shown in Figure 1b. The layer structure of **COF-LZU1** was also observed through scanning electron microscopy (SEM) and transmission electron microscopy (TEM). The SEM image of **COF-LZU1** (Figure 3a) shows the layered-sheet morphology and the boundaries of the TEM images (Figure 3c and Figure S19, SI) show the layered-sheet arrangement of **COF-LZU1**. The formation of the eclipsed structure originates from the strong tendency for the hexagonal units to form coplanar aggregates which could stabilize the $\pi-\pi$ stacking interactions between adjacent layers (distance of ~3.7 Å).

The atomic-level construction of **COF-LZU1** was eventually verified by solid-state NMR spectroscopy. Figure 4a shows the ^{13}C cross-polarization magic-angle spinning (CP/MAS) NMR spectrum recorded for **COF-LZU1**. The ^{13}C NMR peak at ~157 ppm corresponds to the carbon atom of the C=N bond, the formation of which[36] is characteristic for the condensation reaction of aldehyde **1** and primary amine **2**. The signals at ~122, 130, 137, and 148 ppm can be assigned to the carbon atoms of the phenyl groups, while the minor peak at ~191 ppm is ascribed to the carbon atoms of terminal aldehyde groups in the **COF-LZU1** network.

As mentioned above, being highly selective and sensitive toward the incorporation of various metal ions, the imine-type ligand is one of the most versatile ligands studied in coordination chemistry.[31] Moreover, the imine-based metal complexes have also been used as homogeneous catalysts.[37] Recently, amorphous triazine-based frameworks were successfully applied as heterogeneous supports for noble metal catalysts.[38−40] We were thus intrigued to explore the unprecedented possibility of utilizing COF materials in catalysis. Through a simple post-treatment of **COF-LZU1** with palladium acetate (Figure 1a), a Pd(II)-containing **COF-LZU1** material, **Pd/COF-LZU1**, was facilely prepared (see SI for details). A comparison of the PXRD patterns (Figure 5) of **COF-LZU1** and **Pd/COF-LZU1** revealed that the crystal structure of **COF-LZU1** was well preserved after the
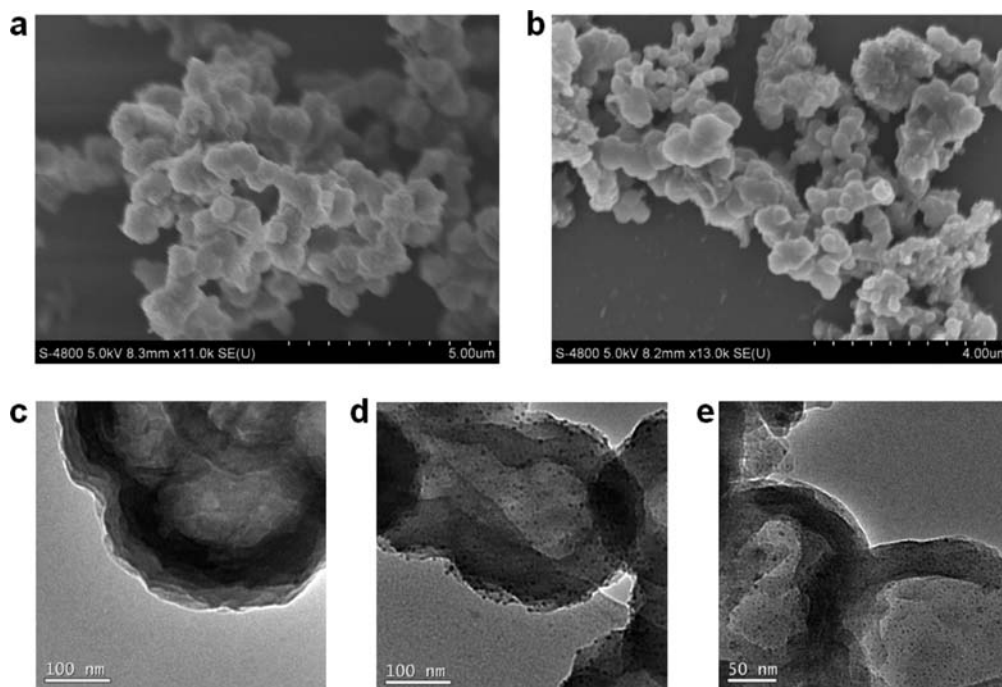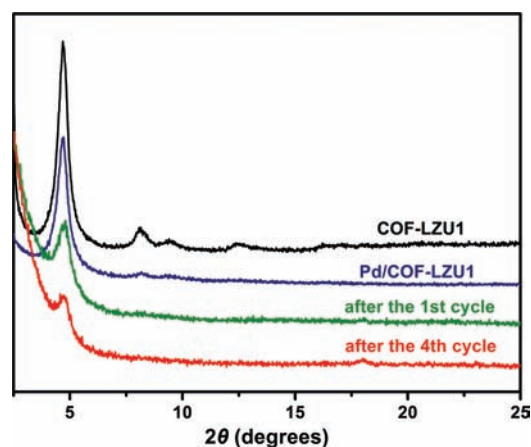
Figure 3. SEM images of **COF-LZU1** (a) and **Pd/COF-LZU1** (b), TEM images of **COF-LZU1** (c), **Pd/COF-LZU1** (d), and **Pd/COF-LZU1** after the fourth cycle use (e). The magnified pictures are shown in the SI for better visuality.
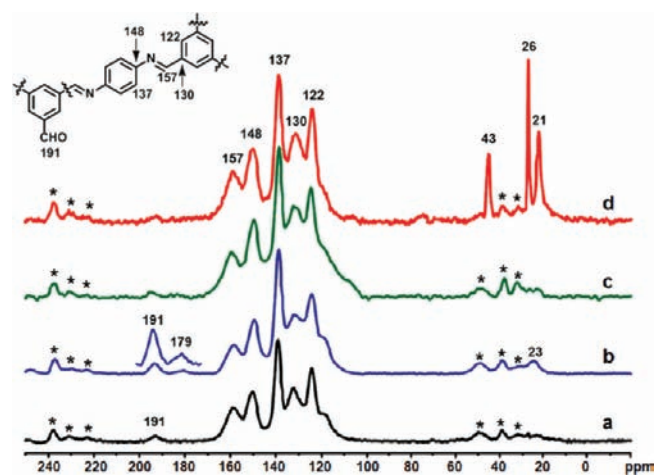
Figure 4. ^{13}C CP/MAS NMR spectra of **COF-LZU1** (a, black), **Pd/COF-LZU1** (b, blue), **Pd/COF-LZU1** after the first cycle use (c, green) and after the fourth cycle use (d, red). Asterisks denote spinning sidebands. The assignments of ^{13}C chemical shifts of **COF-LZU1** were indicated in the chemical structure. The minor signals at ∼179 and 23 ppm (b) were assigned to the acetate groups of the incorporated $Pd(OAc)_2$. The signals at ∼43, 26, and 21 ppm (d) originated from the solvent.

Figure 5. PXRD patterns of **COF-LZU1** (black), **Pd/COF-LZU1** (blue), **Pd/COF-LZU1** after the first cycle (green) and after the fourth cycle (red).
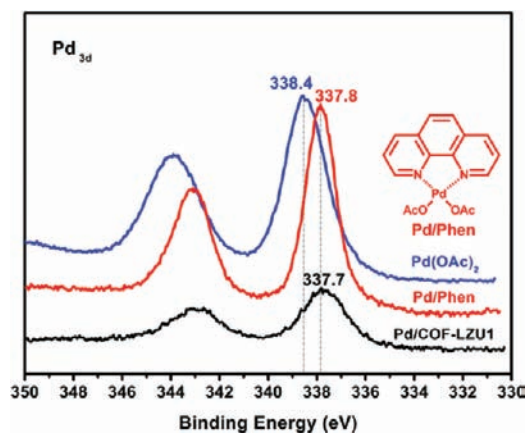
treatment with palladium acetate.[41] The ^{13}C CP/MAS NMR spectrum of **Pd/COF-LZU1** (Figure 4b) is almost identical to that of **COF-LZU1** in the phenyl areas, indicating also the structural preservation of **COF-LZU1** after the post-treatment. Two additional minor peaks at ∼179 and 23 ppm are assigned to the carbonyl and methyl groups of the incorporated $Pd(OAc)_2$. In comparison with those of free $Pd(OAc)_2$ at ∼190 ppm (Figure S27, SI), the ^{13}C chemical shift for the carbonyl group in the incorporated $Pd(OAc)_2$ is high-field

shifted by 11 ppm. This confirms the strong incorporation of $Pd(OAc)_2$ with **COF-LZU1**. As shown in c and d of Figure 3, the layer structure of **COF-LZU1** also remained unchanged after the treatment with palladium acetate. The well-dispersed palladium species (black dots)[42] could also be clearly observed in the TEM images (Figures 3d and S20, SI). The Pd content in **Pd/COF-LZU1** is ∼7.1 ± 0.5 wt % as determined by ICP analysis, corresponding to ∼0.5 Pd atom per unit cell (Figure 1c).

We then performed X-ray photoelectron spectroscopy (XPS) measurements to further investigate the incorporation of palladium within **COF-LZU1**. As shown in Figure 6 (black), the binding energy (BE) of $Pd_{3d5/2}$ in **Pd/COF-LZU1** is 337.7 eV, indicating that the Pd species is present in +2 state.[43] On the other hand, the BE of 337.7 eV for the Pd(II) species in

Figure 6. XPS spectra of free Pd(OAc)$_2$ (blue), **Pd/Phen** (red), and **Pd/COF-LZU1** (black).

Figure 7. Nitrogen adsorption−desorption isotherms of **COF-LZU1** (cycles) and **Pd/COF-LZU1** (triangles). (Inset) Pore size distribution of **COF-LZU1** (cycles) and **Pd/COF-LZU1** (triangles). Adsorption and desorption points are represented by filled and empty symbols, respectively.

Pd/COF-LZU1 shifted negatively by 0.7 eV in comparison with that of 338.4 eV for free Pd(OAc)$_2$ (Figure 6, blue). This negative shift indicates the strong coordination of Pd(OAc)$_2$ with the imine groups of **COF-LZU1**: the imine groups further donate electrons to Pd(II) which makes the Pd species less electron-deficient. In order to further confirm the imine groups between the adjacent layers are indeed incorporating with palladium acetate, a model complex **Pd/Phen** (structure shown in Figure 6) was synthesized from 1,10-phenanthroline (**Phen**) and Pd(OAc)$_2$ (see SI for details). As shown in Figure 6 (red), the XPS spectrum of the coordination complex **Pd/Phen** [with the BE of 337.8 eV for the Pd(II) species] also shows a negative shift of 0.6 eV in comparison with that of free Pd(OAc)$_2$. Moreover, in the ^{13}C CP/MAS NMR spectrum of **Pd/Phen** (Figure S28, SI), the carbonyl group (177 ppm) of the incorporated Pd(OAc)$_2$ also shows a high-field shift by 13 ppm, similar to the case of **Pd/COF-LZU1**. Therefore, Pd(OAc)$_2$ is most probably located in between the adjacent layers of **COF-LZU1** and efficiently coordinated with two nitrogen atoms (distance of ∼3.7 Å) from different layers (Figure 1).
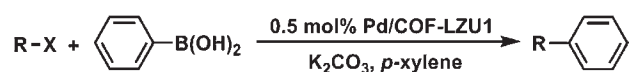
The porosity and surface areas of **COF-LZU1** and **Pd/COF-LZU1** were measured by nitrogen adsorption−desorption analysis at 77 K (Figure 7). The application of the Brunauer−Emmett−Teller (BET) model resulted in the surface areas of 410 and 146 m^2 g^{-1} for **COF-LZU1** (Figure S11, SI) and **Pd/COF-LZU1** (Figure S13, SI), respectively. The total pore volumes were calculated as 0.54 cm^3 g^{-1} ($P/P_0 = 0.99$) and 0.19 cm^3 g^{-1} ($P/P_0 = 0.98$) for **COF-LZU1** and **Pd/COF-LZU1**, respectively. The pore size distributions of **COF-LZU1** and **Pd/COF-LZU1** were calculated using nonlocal density functional theory (NLDFT). As shown in Figure 7 (inset), the pore size distribution plots of both **COF-LZU1** and **Pd/COF-LZU1** revealed a narrow pore width distribution at ∼1.2 nm. In comparison with the case of **COF-LZU1**, the large decrease in the surface area and the slight change in the pore size distribution for **Pd/COF-LZU1** indicate that the presence of palladium acetate would not block the cavities of **Pd/COF-LZU1** but could enhance the weight significantly. The thermogravimetric analysis (Figure S15, SI) identified that both **COF-LZU1** and **Pd/COF-LZU1** possess good thermal stabilities (up to 310 and 270 °C, respectively), which meets the demands for potential applications in catalysis.
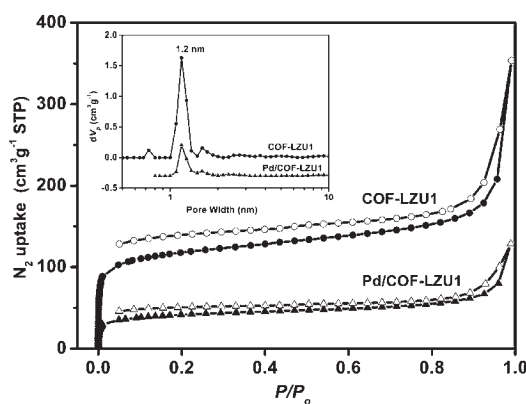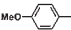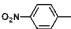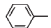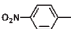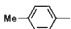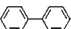
The catalytic activity of **Pd/COF-LZU1** catalyst was examined in one of the representative Pd-catalyzed reactions, *i.e.*, the Suzuki−Miyaura coupling reaction. The Suzuki−Miyaura coupling reaction has been widely applied in homogeneous media for the facile formation of C−C bonds.[32] However, its potential application in industry is still limited due to the diffic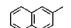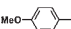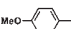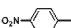ulty in separating and recycling the expensive Pd-catalysts from the product mixture. Using recyclable palladium catalysts is therefore a promising solution to these problems.[44,45] For the purpose of comparison, the Suzuki−Miyaura coupling reaction catalyzed by **Pd/COF-LZU1** was conducted under conditions similar to those for the Pd-containing MOF,[46] and the results are summarized in Table 1. Catalyzed by 0.5 mol % of **Pd/COF-LZU1**, the substituted aryl iodides with either an electron-donating (entry 1) or an electron-withdrawing (entry 2) group afforded the cross-coupling products in excellent yields (96−97%). The less active bromobenzenes (entries 3−8) also gave excellent yields (96−98%) within 2.5−4 h at 150 °C. Furthermore, when 0.1 mol % catalyst was used (entry 10), the reaction also worked well but with a longer reaction time (5 h). All these results clearly indicate that **Pd/COF-LZU1** possesses high catalytic activity in catalyzing the Suzuki−Miyaura coupling reaction. In comparison with the Pd(II)-containing MOF[46] (entry 9), **Pd/COF-LZU1** required less catalyst-loading and shorter reaction time and showed higher reaction yield (entry 8).

We conducted the control experiments to confirm that the reaction was indeed catalyzed by **Pd/COF-LZU1** instead of free Pd(OAc)$_2$. In the absence of reactants, the mixture of **Pd/COF-LZU1**, *p*-xylene and sodium carbonate was heated and stirred for 7 h at 150 °C. The filtrate from the hot mixture was then used to catalyze the reaction of *p*-nitrobromobenzene and phenylboronic acid. No conversion could be observed in this case and the ICP analysis showed that less than 0.08% of Pd content (corresponding to 0.0057 wt % Pd content in **Pd/COF-LZU1**) had leached out into the filtrate. In the presence of reactants, the catalyst was removed from the hot reaction mixture after ∼50% conversion of reactants, and the isolated solution did not exhibit any further reactivity under the same reaction conditions. Moreover, the ICP analysis showed that essentially no Pd (<0.007% Pd content) had leached out into the isolated solution. These studies identified that Pd(OAc)$_2$ is strongly coordinated within **COF-LZU1** under the

**Table 1. Catalytic Activity Test of Pd/COF-LZU1 in the Suzuki–Miyaura Coupling Reaction**

R–X + ⬡–B(OH)$_2$ →(0.5 mol% Pd/COF-LZU1, K$_2$CO$_3$, p-xylene)→ R–⬡

Entry[a]	R	X	Time (h)	Yield (%)[b]
1	MeO–⬡–	I	3	96
2	O$_2$N–⬡–	I	2	97
3	⬡–	Br	3	97
4	O$_2$N–⬡–	Br	3	97
5	Me–⬡–	Br	3	97
6	⬡–⬡–	Br	2.5	98
7	(naphthyl)–	Br	2.5	97
8	MeO–⬡–	Br	4	96
9[c]	MeO–⬡–	Br	5	85
10[d]	O$_2$N–⬡–	Br	5	97

[a] Unless otherwise noted, the reaction conditions are: aryl halide (1.0 mmol), phenylboronic acid (1.5 mmol), K$_2$CO$_3$ (2.0 mmol), and **Pd/COF-LZU1** (0.5 mol %), 4 mL of p-xylene, 150 °C. [b] Isolated yield. [c] Result from ref 46 (2.5 mol % Pd/MOF was used). [d] 0.1 mol % **Pd/COF-LZU1** was used.

applied reaction conditions and that the trace amount of Pd(OAc)$_2$ leaching out could not catalyze the Suzuki–Miyaura reaction.

The recycle use of **Pd/COF-LZU1** catalyst (1.0 mol %) was further examined in the reaction of p-nitrobromobenzene with phenylboronic acid (Table 2). The results demonstrated that **Pd/COF-LZU1** catalyst could be reused at least for four times without loss of catalytic activity and selectivity. The XPS spectra of the recycled **Pd/COF-LZU1** catalyst (Figure S25, SI) show that the Pd species was still present in +2 state. The TEM images of the recycled **Pd/COF-LZU1** catalyst (Figures 3e and S21-[SI]) indicate that the Pd species were still highly dispersed. The comparison of the ^{13}C CP/MAS NMR spectra (Figure 4a–d) and the PXRD patterns (Figure 5) of the **Pd/COF-LZU1** catalysts after different reaction runs indicates that the crystallinity and the atomic-level structure of **Pd/COF-LZU1** was almost maintained, although the intensity of the PXRD pattern was gradually decreased. The decrease of structural regularity should be due to the repetitive exposure of **Pd/COF-LZU1** catalyst to the relatively harsh conditions of the Suzuki–Miyaura reaction (temperature of 150 °C and sodium carbonate as the base).

We infer that the superior activity of **Pd/COF-LZU1** catalyst should be attributed to its unique structure. The eclipsed layered-sheet arrangement of **COF-LZU1** offers a robust scaffold for Pd(OAc)$_2$ incorporation. The distance (~3.7 Å) of eclipsed nitrogen atoms in adjacent layers falls into the ideal requirement for strong coordination of Pd(OAc)$_2$. Moreover, the regular channels with a diameter of ~1.8 nm provide efficient access to the active sites together with fast diffusion for the bulky products. In the case of MOF catalysts, the metal active sites, being also responsible for structural preservation, are surrounded by bulky ligands. Not only would the access to these active sites be limited, but also the involvement of these active sites in catalysis could lose the structural integrity, the case of which has been evidenced

Table 2. Recycle Test of Pd/COF-LZU1 in the Suzuki–Miyaura Cross-Coupling Reaction of p-Nitrobromobenzene and Phenylboronic Acid

O$_2$N–⬡–Br + ⬡–B(OH)$_2$ →(1 mol% Pd/COF-LZU1, K$_2$CO$_3$, p-xylene)→ O$_2$N–⬡–⬡
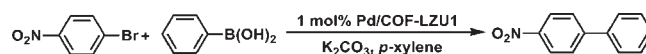
entry	time (h)	yield (%)[a]
fresh	3	97
cycle 1	3	96
cycle 2	3	97
cycle 3	3	97
cycle 4	3	97

[a] Isolated yield.

by the moderate activity and relatively poor recyclability of Pd(II)-containing MOF catalyst in the Suzuki–Miyaura reaction.[46] In the case of zeolite catalysts, a general problem[12] is that the structural topology and small pore/channel size (normally <0.8 nm) would cause severe diffusion problems, restricting their catalytic applications for bulky systems. Moreover, further decrease of the void space makes the postmodified zeolites less applicable for catalysis, especially for fine chemical catalysis.

■ CONCLUSION

In conclusion, for the purpose of catalytic applications, we have successfully constructed an imine-based COF material, **COF-LZU1**, from simple starting materials. The two-dimensional layered-sheet structure together with the eclipsed imine bonds render the **COF-LZU1** material as an ideal scaffold for coordinating metal ions. Accordingly, the robust incorporation of Pd(OAc)$_2$ into **COF-LZU1** was realized with a simple post-treatment and verified by spectroscopic analyses. The synthesized **Pd/COF-LZU1** material was further applied to catalyze the Suzuki–Miyaura coupling reaction, an important reaction for the formation of C–C bonds. The superior activity of **Pd/COF-LZU1** catalyst was testified by the broad scope of the reactants, the excellent yields of the reaction products, and the high stability and easy recyclability of the catalyst. In comparison with other crystalline porous materials (zeolites and MOFs), the unique structure of **Pd/COF-LZU1** provides efficient access to the catalytic sites and fast mass-transport of the reactants/products, which are responsible for its superior activity in catalyzing the Suzuki–Miyaura coupling reaction.

In this contribution, not only is the first example of utilizing COF material for catalysis demonstrated but also the tolerance of **COF-LZU1** in relatively harsh reaction conditions is verified. It is therefore believed that the **COF-LZU1** scaffold could act as a stable, robust, and versatile "supramolecular ligand" and host a variety of metal ions for catalyzing a wide scope of reactions, even at harsh reaction conditions. Also, we expect that our approach will boost the research on employing functional COF materials for catalysis, the further progress of which may eventually bring COF materials into industrial applications.

■ ASSOCIATED CONTENT

S **Supporting Information.** Detailed synthetic procedures, FT-IR spectra, PXRD patterns, modeling details and atomic coordinates, gas adsorption, TGA traces, SEM images, TEM images,

XPS spectra, and ^{13}C CP/MAS NMR spectra. This material is available free of charge via the Internet at http://pubs.acs.org.

■ AUTHOR INFORMATION

Corresponding Author
wang_wei@lzu.edu.cn

■ ACKNOWLEDGMENT

■ REFERENCES

(1) Yaghi, O. M.; O'Keeffe, M.; Ockwig, N. W.; Chae, H. K.; Eddaoudi, M.; Kim, J. *Nature* **2003**, *423*, 705.

(2) Côté, A. P.; Benin, A. I.; Ockwig, N. W.; O'Keeffe, M.; Matzger, A. J.; Yaghi, O. M. *Science* **2005**, *310*, 1166.

(3) El-Kaderi, H. M.; Hunt, J. R.; Mendoza-Cortes, J. L.; Côté, A. P.; Taylor, R. E.; O'Keeffe, M.; Yaghi, O. M. *Science* **2007**, *316*, 268.

(4) Côté, A. P.; El-Kaderi, H. M.; Furukawa, H.; Hunt, J. R.; Yaghi, O. M. *J. Am. Chem. Soc.* **2007**, *129*, 12914.

(5) Hunt, J. R.; Doonan, C. J.; LeVangie, J. D.; Côté, A. P.; Yaghi, O. M. *J. Am. Chem. Soc.* **2008**, *130*, 11872.

(6) Tilford, R. W.; Gemmill, W. R.; zur Loye, H. C.; Lavigne, J. J. *Chem. Mater.* **2006**, *18*, 5296.

(7) Tilford, R. W.; Mugavero, S. J.; Pellechia, P. J.; Lavigne, J. J. *Adv. Mater.* **2008**, *20*, 2741.

(8) Čejka, J.; Corma, A.; Zones, S. *Zeolites and Catalysis: Synthesis, Reactions and Applications*; Wiley-VCH: New York, 2010.

(9) Eddaoudi, M.; Moler, D. B.; Li, H. L.; Chen, B. L.; Reineke, T. M.; O'Keeffe, M.; Yaghi, O. M. *Acc. Chem. Res.* **2001**, *34*, 319.

(10) James, S. L. *Chem. Soc. Rev.* **2003**, *32*, 276.

(11) Thomas, A. *Angew. Chem., Int. Ed.* **2010**, *49*, 8328.

(12) Corma, A. *Chem. Rev.* **1997**, *97*, 2373.

(13) Corma, A.; Garcia, H.; Xamena, F. X. L. *Chem. Rev.* **2010**, *110*, 4606.

(14) Mastalerz, M. *Angew. Chem., Int. Ed.* **2008**, *47*, 445.

(15) Kuhn, P.; Antonietti, M.; Thomas, A. *Angew. Chem., Int. Ed.* **2008**, *47*, 3450.

(16) Uribe-Romo, F. J.; Hunt, J. R.; Furukawa, H.; Klock, C.; O'Keeffe, M.; Yaghi, O. M. *J. Am. Chem. Soc.* **2009**, *131*, 4570.

(17) Campbell, N. L.; Clowes, R.; Ritchie, L. K.; Cooper, A. I. *Chem. Mater.* **2009**, *21*, 204.

(18) Dogru, M.; Sonnauer, A.; Gavryushin, A.; Knochel, P.; Thomas, B. *Chem. Commun.* **2011**, *47*, 1707.

(19) Colson, J. W.; Woll, A. R.; Mukherjee, A.; Levendorf, M. P.; Spitler, E. L.; Shields, V. B.; Spencer, M. G.; Park, J.; Dichtel, W. R. *Science* **2011**, *332*, 228.

(20) Furukawa, H.; Yaghi, O. M. *J. Am. Chem. Soc.* **2009**, *131*, 8875.

(21) Doonan, C. J.; Tranchemontagne, D. J.; Glover, T. G.; Hunt, J. R.; Yaghi, O. M. *Nature Chem.* **2010**, *2*, 235.

(22) Assfour, B.; Seifert, G. *Microporous Mesoporous Mater.* **2010**, *133*, 59.

(23) Wan, S.; Guo, J.; Kim, J.; Ihee, H.; Jiang, D. L. *Angew. Chem., Int. Ed.* **2008**, *47*, 8826.

(24) Wan, S.; Guo, J.; Kim, J.; Ihee, H.; Jiang, D. L. *Angew. Chem., Int. Ed.* **2009**, *48*, 5439.

(25) Spitler, E. L.; Dichtel, W. R. *Nature Chem.* **2010**, *2*, 672.

(26) Spitler, E. L.; Giovino, M. R.; White, S. L.; Dichtel, W. R. *Chem. Sci.* **2011**, *2*, 1588.

(27) Li, Y. W.; Yang, R. T. *AIChE J.* **2008**, *54*, 269.

(28) Jiang, J. X.; Cooper, A. I. *Top. Curr. Chem.* **2010**, *293*, 1.

(29) Lanni, L. M.; Tilford, R. W.; Bharathy, M.; Lavigne, J. J. *J. Am. Chem. Soc.* **2011**, *133*, 13975.

(30) Uribe-Romo, F. J.; Doonan, C. J.; Furukawa, H.; Oisaki, K.; Yaghi, O. M. *J. Am. Chem. Soc.* **2011**, *133*, 11478.

(31) Singh, G.; Singh, P. A.; Sen, A. K.; Singh, K.; Dubey, S. N.; Handa, R. N.; Choi, J. H. *Synth. React. Inorg. Met.-Org. Chem.* **2002**, *32*, 171.

(32) Miyaura, N.; Suzuki, A. *Chem. Rev.* **1995**, *95*, 2457.

(33) Materials Studio Release Notes v.4.4 (Accelrys Software, San Diego, 2008).

(34) As addressed in a recent work (ref 30), Rietveld refinement, which can determine precisely the framework topology, is not applicable in the cases of COF materials due to the low resolution of the PXRD patterns. Pawley refinement, which is being used for COF systems, could not offer the unique assignment for the packing issue based on the unit cell and the space group only. Accordingly, although the simulated PXRD pattern via Pawley refinement does not match the observed data, the staggered-packing structure cannot be absolutely ruled out.

(35) Lukose, B.; Kuc, A.; Heine, T. *Chem.—Eur. J.* **2011**, *17*, 2388.

(36) Pandey, P.; Katsoulidis, A. P.; Eryazici, I.; Wu, Y. Y.; Kanatzidis, M. G.; Nguyen, S. T. *Chem. Mater.* **2010**, *22*, 4974.

(37) Martell, A. E.; Perutka, J.; Kong, D. *Coord. Chem. Rev.* **2001**, *216*, 55.

(38) Palkovits, R.; Antonietti, M.; Kuhn, P.; Thomas, A.; Schüth, F. *Angew. Chem., Int. Ed.* **2009**, *48*, 6909.

(39) Chan-Thaw, C. E.; Villa, A.; Katekomol, P.; Su, D.; Thomas, A.; Prati, L. *Nano Lett.* **2010**, *10*, 537.

(40) Chan-Thaw, C. E.; Villa, A.; Prati, L.; Thomas, A. *Chem.—Eur. J.* **2011**, *17*, 1052.

(41) The PXRD patterns of **Pd/COF-LZU1** and **COF-LZU1** showed subtle differences only. Therefore, the incorporation of ~0.5 $Pd(OAc)_2$ per unit cell does not affect the layered structure of **COF-LZU1** but may slightly change the initial layer space (3.7 Å) of **COF-LZU1**.

(42) As overwhelmingly demonstrated by the XPS and solid-state NMR studies, the palladium species incorporated in **Pd/COF-LZU1** is $Pd(OAc)_2$ with the Pd in +2 state. However, the black dots observed in the TEM images of **Pd/COF-LZU1** (d and e of Figure 3 and Figures S20 and S21(SI)) are attributed to the Pd(0) nanoparticles formed upon the electron-beam induced reduction of the original Pd(II) species during the TEM measurements. This phenomenon has previously been noticed and explained by other groups. For example, Wahl *et al.* observed the formation of palladium nanoparticle arrays from K_2PdCl_4 which was initiated by the electron beam in the TEM. Wahl, R.; Mertig, M.; Raff, J.; Selenska-Pobell, S.; Pompe, W. *Adv. Mater.* **2001**, *13*, 736. Stark *et al.* found the metalization of $Pd(OAc)_2$ films induced by electron-beam. Stark, T. J.; Mayer, T. M.; Griffis, D. P.; Russell, P. E. *J. Vac. Sci. Technol., B* **1991**, *9*, 3475. *J. Vac. Sci. Technol., B* **1992**, *10*, 2685. We also found that the black dots were absent in the TEM images of $Pd(OAc)_2$-free **Phen** sample (Figure S22, SI), but showed up in those of $Pd(OAc)_2$-coordinated **Pd/Phen** sample (Figure S23, SI) and of pure $Pd(OAc)_2$ sample (Figure S24, SI). These observations further verified the origin of Pd(0) species.

(43) Thomas, A. C. *Photoelectron and Auger Spectroscopy*; Plenum: New York, 1975.

(44) Magano, J.; Dunetz, J. R. *Chem. Rev.* **2011**, *111*, 2177.

(45) Arpad, M. *Chem. Rev.* **2011**, *111*, 2251.

(46) Xamena, F.; Abad, A.; Corma, A.; Garcia, H. *J. Catal.* **2007**, *250*, 294.